We are IntechOpen,
the world's leading publisher of
Open Access books
Built by scientists, for scientists

4,500
Open access books available

119,000
International authors and editors

135M
Downloads

Our authors are among the

154
Countries delivered to

TOP 1%
most cited scientists

12.2%
Contributors from top 500 universities

CLARIVATE ANALYTICS

BOOK
CITATION
INDEX

INDEXED

WEB OF SCIENCE™

Selection of our books indexed in the Book Citation Index
in Web of Science™ Core Collection (BKCI)

Interested in publishing with us?
Contact book.department@intechopen.com

Controlled Mixing and Transport in Comb-Like and Random Jet Array Stirring Systems

S. Delbos[1], E. Chassaing[1], P. P. Grand[2],
V. Weitbrecht[3] and T. Bleninger[4]

[1]*Institute for Research and Development of Photovoltaic Energy (IRDEP),
UMR 7174 EDF - CNRS - Chimie-ParisTech*
[2] *Nexcis*
[3] *VA f. Wasserbau/Hydrologie/Glaziologie ETH Zürich*
[4]*Institute for Hydromechanics, Karlsruhe Institute of Technology (KIT)*
[1,2]*France*
[3]*Switzerland*
[4]*Germany*

1. Introduction

Electrodeposition of alloys from low concentrated solutions or solutions whose elements have very different redox potentials is often strongly dependent on mass-transfer rate of one of the electroactive species. For such alloy systems, electrodeposition is carried out potentiostatically because the deposition potential has to be controlled in order to monitor good alloy composition. The applied potential is such that one of the species is deposited at its diffusion limiting current, and the other is deposited under activation-controlled regime. The diffusion layer's thickness controls the limiting current, and its uniformity controls the uniformity of the deposited film (Bard & Faulkner, 2001).

In electronical engineering, the paddle-cell system has been used for a long time to enhance mass-transfer rate and homogeneity (Powers & Romankiw, 1972). It can be used for different electrochemical systems (Datta & Landolt, 2000). The paddle-cell system, where a paddle-like object is moved back and forth continuously through the solution, has been used for a long time in electronical engineering to enhance mass transfer rate and homogeneity. It can be used for different electrochemical systems such as Pb-Sn (Datta & Landolt, 2000) or Fe-Ni (Powers & Romankiw, 1972). The paddle system is widely used in industry (McHugh et al., 2005; Keigler et al., 2005), but few studies deal with improving the process conditions in relationship with mean and local mass transfer.

A comb-like stirring system has been developed at IRDEP. It is similar to the paddle system and the shear plate system (Wu et al., 2005). The comb can be considered as an improvement of the paddle system by having several paddles one after another in a comb like arrangement. The comb is moved back and forth continuously through the solution. It is used for enhancing the homogeneity of electrodeposited Cu-In-Se layers that are the main component of CIS thin-film photovoltaic devices (Lincot et al., 2004).

Another system, the jet array, can also be used to plate Ni-Fe (permalloy) static wafers (Tzanavaras & Cohen, 1995). Hereby no moving parts pass through the solution, but the

solution itself is pumped through small openings causing jet mixing in the system. An improvement of this system was investigated.

The mixing and transport processes are described for each stirring system. Firstly, the paddle system characteristics are described based on a literature review. Secondly, the comb system will be introduced by describing the performed experiments and results, as well as proposing characteristic non-dimensional numbers for design purposes. Thirdly, the randomly firing jet array system will by analysed and parametrized based on the experimental results obtained from (Delbos et al., 2009b;a), which also describe the experimental details of their experiments, but which will not be repeated here.

2. Paddle-cell system

The paddle-cell, which is quite similar to the comb-like system, is well documented and can provide insight for comb-like system development. The paddle-cell was first developed by IBM (Powers & Romankiw, 1972) to provide laminar agitation and to improve mass transfer during copper electrodeposition. A paddle goes back and forth (reciprocates) above a horizontal cathode (fig. 1). Experimental data (Schwartz et al., 1987; Rice et al., 1988) and numerical simulations (Wilson & McHugh, 2005; Mandin et al., 2007) show that geometrical parameters of the paddle, size and aspect ratio of the cell and paddle shape have a strong influence on mass-transfer phenomena within the electrochemical cell.

In literature a relationship has been proposed between the diffusion layer thickness and paddle geometrical parameters. The Sherwood number, which can be defined as the ratio of the advection lengthscale and the diffusion lengthscale, was shown to be equal to:

$$Sh = \frac{\text{Advection lengthscale}}{\text{Diffusion lengthscale}} = \frac{g+h}{\delta} = \alpha Re^m Sc^{1/3} \qquad (1)$$

where m and α are coefficients that depend on the geometry of the system, $Re = V \cdot (h+g)/\nu$, $Sh = (h+g)/\delta$, $Sc = \nu/D$. In the case of the paddle-cell, the advection lenghtscale is $g+h$, because the size of the eddies is determined by the smallest dimension available to them. The two other dimensions (heigth of the fluid and dimension of the cell in the direction parallel to the comb movement) are clearly bigger.

When Sherwood, Reynolds and Schmidt numbers can be linked by such a relationship, the diffusion layer thickness δ, through the Sherwood number, is totally controlled by the geometrical parameters of the tank. The value of m depends on turbulence intensity : $m \sim 0.5$ denotes laminar flow, $m \sim 0.75$ denotes turbulent flow (Bard & Faulkner, 2001; Cussler, 1997;
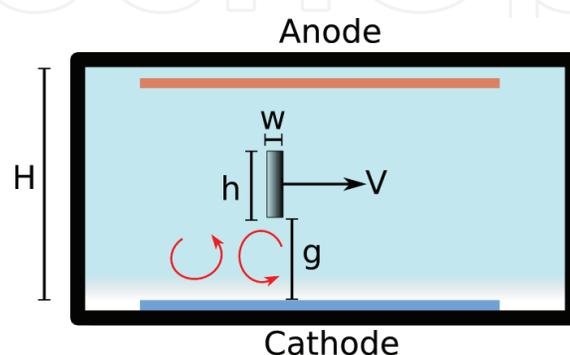

Fig. 1. Schematic view of a paddle-cell from above

Tennekes & Lumley, 1972; Brumley & Jirka, 1988). This type of analysis was also used for other systems, for example the shear flow system (Wu et al., 2005).

Numerical simulations were performed by (Wilson & McHugh, 2005) proposing a modification of equation 1 by including further characteristical numbers to describe the physical meaning of the previous used coefficients. In Wilson and McHugh's paper, three adimensional numbers have been introduced : the blockage ratio h/H, the proximity ratio h/g, the Strouhal number $f_v h/u_B$, where f_v is the vortex shedding frequency and u_B is the eddy velocity:

$$Sh = 0.566 Re^{0.583} \left(\frac{h}{g}\right)^{0.151} \left(\frac{h}{H}\right)^{0.168} St^{0.283} Sc^{1/3} \qquad (2)$$

The insight provided by these studies was useful for chosing relevant geometric parameters and designing characteristic non-dimensional parameters.

3. Comb-like system

3.1 Electrochemical reactor

A comb-like system is used for stirring. It is a piece of chemically inert material such as PP, PTFE or PVDF that has the shape of a comb. It is located in front of the cathode and it reciprocates in the direction parallel to the cathode, thus creating turbulence near the cathode (fig. 2). It has the advantages of simplicity and easy maintenance, but the drawback of a built-in anisotropy: the teeths create vertical patterns on the electrodeposited layer.

A modular tank was built to analyze the influence of the hydrodynamical parameters on a Cu-Ni electrodeposition process. In this tank local flow velocities have been measured in high temporal resolution using Laser Doppler Velocimetry (LDV). In addition, electrodeposition of Cu-Ni alloy films has been carried out on 5 x 5 cm^2 glass–Mo substrates.

The experimental tank allowed the study of a wide range of parameter variations (table 1). Results from studies on the paddle-cell (Schwartz et al., 1987; Rice et al., 1988; Wilson & McHugh, 2005) suggest that the most important parameters should be the distance between the comb and the cathode (g, see figure 2), the stirring frequency (f) and stroke (S, maximum amplitude of stirring), the width of the comb (h), the shape of the teeth section, and the dimensions of the cell (L and H). Prior unpublished studies also showed that the mesh of the comb (M) could have an influence on the hydrodynamical conditions.
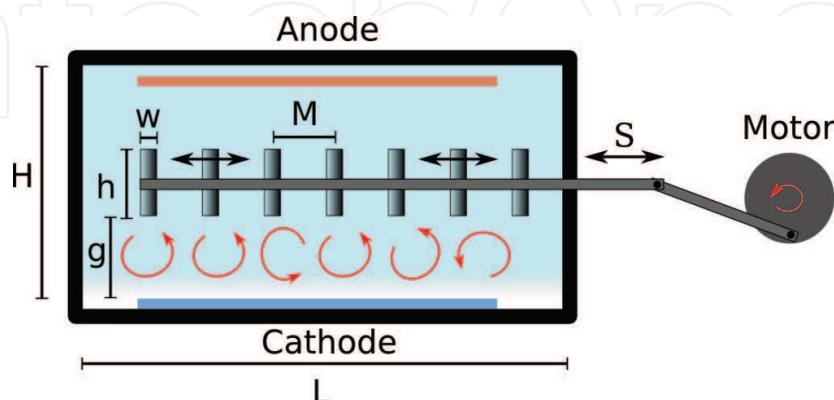

Fig. 2. Schematics of a comb-like system seen from above.

Parameter	Range
g (mm)	$4 - 500$
M (mm)	$3 - 16$
w (mm)	$1 - 8$
h (mm)	$1 - 20$
S (mm)	≤ 40
f (Hz)	≤ 7
Tooth section	rectangular circular triangular double triangle
H	$10 - 500$ mm
L	$150 - 700$ mm

Table 1. Hydrodynamical conditions of the comb-like system.

3.2 Electrodeposition

In order to investigate mass-transport phenomena, an electrochemical model system was developed in the laboratory (Ollivier et al., 2009). This system, the Cu-Ni system is an appropriate model: copper deposition is controlled by mass transfer phenomena, while nickel deposition is controlled by charge-transfer. Its deposition kinetics is a simplification of the Cu-In-Se codeposition system that is used for synthetizing solar cells in the laboratory, but easier to handle.

For the preparation of large volumes of Cu-Ni electrolyte (~ 40 L), the chemicals ($NiSO_4$ 0.165 M, $CuSO_4$ 0.025 M, Sodium Citrate 0.25 M) were first dissolved in smaller volumes (2 x 5 L), and immediately diluted into the whole water volume, to prevent the caking (mass precipitation) of the 40 L-electrolyte.

The electrodeposition takes place on a glass substrate covered with a sputtered Mo layer. The resistivity of the Mo layer is $\rho_{ca} = 13 - 17 \ \mu\Omega.cm$, its thickness $e = 0.38 - 0.52 \ \mu$m and its sheet resistance is $= 0.27 - 0.44 \ \Omega$. This is the usual substrate for thin layer solar cells (Lincot et al., 2004).

The substrate is placed in an adapted basket that allows the substrate to be carried through the cleaning process. The substrate is first rinsed with high-purity water (18.2 MΩ), cleaned with soaped water and thoroughly rinsed with high-purity water. Finally it is dipped for 10 minutes into a NH_3 solution (25 %) to deoxidize the Mo (mainly to remove MoO_2). The substrate is afterwards rinsed with flowing water, and dried with argon.

The electrodeposition is performed in potentiostatic mode. The counter-electrode is a vertical 5 x 15 cm^2 Ti mesh covered with IrO_2 (Dimensionally stable Anode, DSA). A saturated Mercurous Sulfate Electrode (MSE, +0.65 V / Normal Hydrogen Electrode) is used as a reference electrode. The potentiostat is an Autolab PGSTAT30 controlled by the GPES software running under MS Windows.

A Pt wire is applied on the substrate to achieve the electrical contact, the substrate is then rinsed with flowing water, just before being dipped in the electrolyte. The substrate is then immersed and the potential of -1.60 V/MSE is applied, and the total charge is -2.8 C/cm^2 The resulting electrodeposited layers are composed of 90 - 99 % of copper and 1 - 10 % of nickel. This composition is the same as in similar experiments performed in a jet firing array system (Delbos et al., 2009a).

3.3 Chemical analysis

The thickness and chemical composition of the layers were analysed by Energy-Dispersive Spectroscopy X-Ray Fluorescence Fischerscope Xray Xan controlled by the WinFTM software running under Windows. The uncertainty of the measurement was 0.26 % for the thickness, 0.04 % for the copper content, 5.73 % for the nickel content. The local electrodeposited copper quantity $n_{Cu}(x,y)$ (in mol/cm^2) is linked to the local diffusion layer thickness $\delta(x,y)$ by this relationship:

$$n_{Cu(x,y)} = \frac{i_{Cu}(x,y)t}{\rho_{Cu}z_e F} = \frac{C_{Cu}D_{Cu}t}{\delta(x,y)} \quad (3)$$

where $i_{Cu}(x,y)$ is the local copper partial current density, t is the electrodeposition time, $z_e = 2$ is the number of electrons involved in the reaction, F is the Faraday's constant, ρ_{Cu} is the per volume ratio of Cu, C_{Cu} is the concentration of Cu^{II} species in the electrolyte, and D_{Cu} is the diffusion coefficient of Cu^{II} species.

The copper quantity is therefore locally dependent on the local diffusion layer thickness. In this set of experiments, mappings of $n_{Cu(x,y)}$ were performed: 5 rows of 20 measurements. Each row (parallel to the x direction) has a resolution of 2.5 mm, and each row is 10.75 mm from its neighbors. The standard deviation of these measurements is therefore a good indication on the spatial variations of the diffusion layer thickness.

Because of flaking on the edges of the plates, the standard deviation is calculated on the three central rows of measurements.

3.4 Laser Doppler Velocimetry

Velocity measurements have been performed using a 2-D Laser Doppler Velocimetry (LDV) system to determine the mean and turbulent flow characteristics. Such a device was already used to correlate flow velocity with electrodeposition patterns in a jet-firing plating cell (Delbos et al., 2009a;b). A 5 W Ar-Ion laser, a Dantec data acquisition apparatus (FiberFlow 60*81 BSA 55X) and the BSA Flow software running under MS Windows were used for data acquisition. ZrO$_2$ particles were used as seeding particles, and they were approximately 3 μm in diameter.

A backscatter probe with a focal length of 310 mm was used. The system provides a temporal resolution of the order of 10^{-2} s and the size of the measurement volume is about 0.1 mm x 0.1 mm x 1.6 mm.

The laser probe was located above the measurement volume, firing in the y-direction, and the laser had to cross the free air-water interface. In order to keep the interface horizontal, a small piece of glass is kept at the air-water interface above the measurement volume. The lack of this piece of glass, or the presence of a drop of water on the piece of glass could lead the acquisition data frequency to decrease by a factor of 100.

Each measurement series lasted 120 - 150 s, leading to approximately 2,000 - 3,000 velocity signals at each point before moving to another point of measurement. Measurements were taken on a horizontal line at a distance $z_m = 2$ mm away from the deposition electrode and 70 mm from the bottom of the tank (total fluid depth: 120 mm). With the help of a 2-D traversing system the LDV probe was positioned at the different measurement locations. The set-up is schematized on figure 3.

u and w, the velocity components on the x- and z-directions were measured. Simple treatment was applied to the data: for each point of measurement, in both measured velocity directions (u in the x-direction and w in the z-direction), the mean velocity and the Root Mean Square
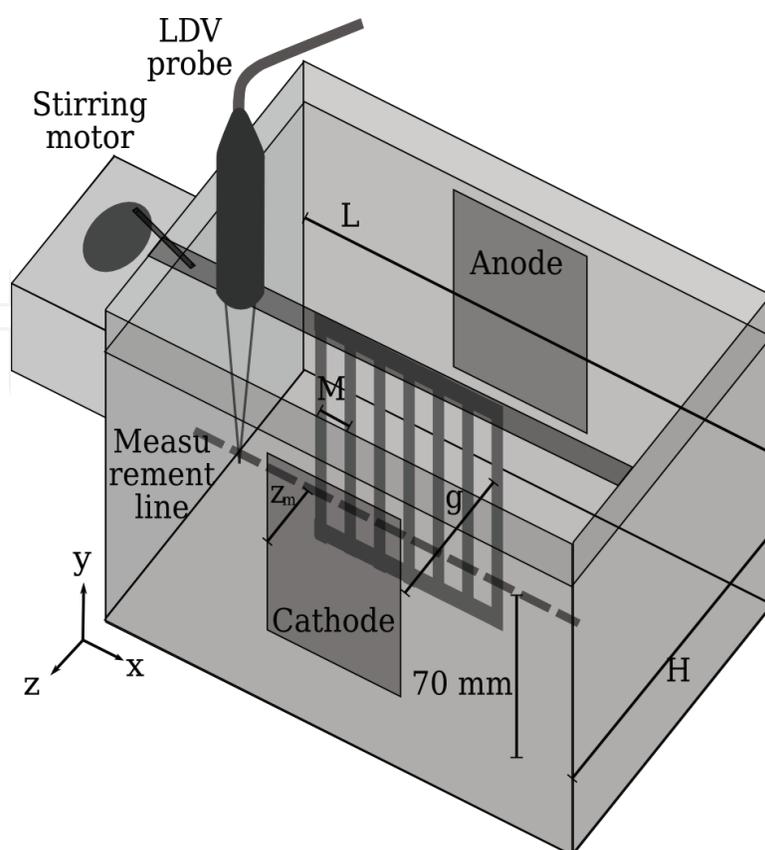
Fig. 3. Schematics of the LDV measurement set-up in the comb experiment.

(RMS) velocity were calculated, e.g. for w:

$$\overline{w} \qquad = \frac{1}{N}\sum_i w_i \text{ is the mean velocity} \tag{4}$$

$$w_{\text{RMS}} \quad = \sqrt{\frac{1}{N}\sum_i (w_i - \overline{w})^2} \text{ is the RMS velocity} \tag{5}$$

where each w_i is one measurement in a series of N measurements. In the following, the RMS velocity is also called the *turbulent fluctuations*.

The uncertainty of the mean and RMS velocity measurements was determined by measuring the velocity at the same point 30 times and then calculating the normalized standard deviation of the measurements ($\sigma_{\text{norm}} = \sigma/\mu$, see section 3.3). The uncertainty of measurement is high for the w component ($\sigma_{\overline{w}}$ = 13.2 %), but it is more acceptable for the u component ($\sigma_{\overline{u}} < 5\%$). These values are summarized in table 2.

4. Results : control parameters of Cu-Ni electrodeposition in comb-like systems

The objective was to define two control parameters for the comb-like system: one that controls the limiting deposition current i_L on the whole cathode, the other that controls the standard deviation of electrodeposited copper σ_{Cu} on a horizontal line (x direction) on the cathode.

Measurement	$\overline{u}$	$\overline{w}$	u_{RMS}	w_{RMS}
σ	4.2 %	13.2 %	4.1 %	7.1 %

Table 2. Uncertainty of LDV measurements in the modular comb electrolyser.

S (mm)	10	14	24
σ_{Cu}	13.32	8.87	3.73

Table 3. Stroke – Cu standard deviation.

Therefore, the effect of the variation of geometrical parameters on the limiting current and the homogeneity of the electrodeposited layer was studied. From these results the two control parameters were defined.

A set of experiments, previously described in (Delbos, 2008), were performed in order to quantify the effect of each geometric parameter on copper deposition and flow parameters. Geometric parameters f, S, M, g, H, and L were tested for relevance (see fig.2). In contrary to the paddle-cell, the flow is confined between the comb and the cathode, leading to a characteristic size of flow vortices (eddy size) $u_B \sim g$. Consequently the parameters H and L do not seem to have an influence on flow velocity and electrodeposition pattern. Only f, S, M, g and teeth shape are found as relevant parameters (Delbos, 2008).

4.1 Effect of the variation of the stroke on electrodeposition and flow

In this section, the effect of the variation of the stroke of the comb is shown. In this set of experiments all parameters but the stroke remain constant ($H = 66$ mm, $L = 310$ mm, $M = 7$ mm, $h = 4$ mm, $g = 7$ mm, $f = 4$ Hz, $w = 1$ mm, the shape of the teeth was rectangular). The stroke S is varied from 10 mm to 24 mm. Fig. 4 shows the results: (a) presents the copper quantity measured by XRF along the horizontal axis of the cathode, (b) and (c) present the mean flow and the turbulent fluctuations measured at $z_m = 2$ mm from the cathode on an axis parallel to the axis were the copper quantity was measured.

The increase of the stroke at constant frequency increases the velocity of the comb, and therefore the energy input. Consequently the turbulent fluctuations increase with comb stroke (fig 4(c)), leading to increased mass transfer and increased deposited copper quantity (fig 4(a)). Increasing the stoke also increases the variations of mean flow (fig 4(b), but apparently the strong variations of the mean flow do not lead to inhomogeneous diffusion layer thickness: the copper quantity is more homogeneous for high values of S (table 3 and fig. fig 4(a)).

4.2 Non-dimensional parameters

From the same kind of experiments that are shown in section 4.1 and the literature (Wilson & McHugh, 2005; Schwartz et al., 1987; Rice et al., 1988), relevant non-dimensional parameters were chosen to characterize the comb-like system:

– non-dimensional stroke S/M

   In this system, each tooth of the comb behaves as a simple paddle, but the vortices shed by each tooth interact with the vortices shed by the neighboring tooth. The non-dimensional stroke S/M is therefore of primary importance for mass-transfer phenomena.

– Proximity ratio h/g

   For grid stirring devices, the turbulent fluctuations (RMS) decay proportionally to the inverse of the distance from the stirring device (at the cathode surface, $u_{RMS} \propto g^{-1}$) (Thompson & Turner, 1975). For the comb system, the energy input is proportionnal to the volume of fluid displaced by the comb, which is proportional to h, and its decay should be proportional to the distance between comb and cathode g. The proximity ratio (h/g) was therefore chosen as a relevant parameter for the system.

– Reynolds number

   For the paddle cell, $Re = (g+h)fS/\nu$. The same definition was chosen for the comb system.

In our experiments, $100 < Re < 4000$. Nevertheless LDV measurements showed that the flow was turbulent even for low Reynolds numbers ($u_{RMS}/\overline{u} \sim 2$, see fig. 4).

– Solidity ratio M/w
   For grid-stirring devices, a solidity ratio can be computed, it is equal to the surface of the grid divided by the surface of the holes (Thompson & Turner, 1975). Similarly the solidity ratio of a comb-like system is M/w: the solution volume displaced by the comb depends on this mesh size over tooth thickness ratio. The larger this ratio, the bigger the volume displaced by the comb, and the more energy is introduced in the system.

– The Schmidt number $Sc = \nu/D$
   In these experiments, the diffusion coefficient is $D = 3 \cdot 10^{-10} \text{m}^2/\text{s}$ and the kinematic viscosity is $\nu = 1.62 \cdot 10^{-6} \text{m}^2/\text{s}$ (Henninot, 1999), leading to $Sc = 5.4 \cdot 10^3$.

4.3 Deposition current control

In case of diffusion-controlled reactions, the current can be linked to the diffusion layer thickness through the classical relationship:
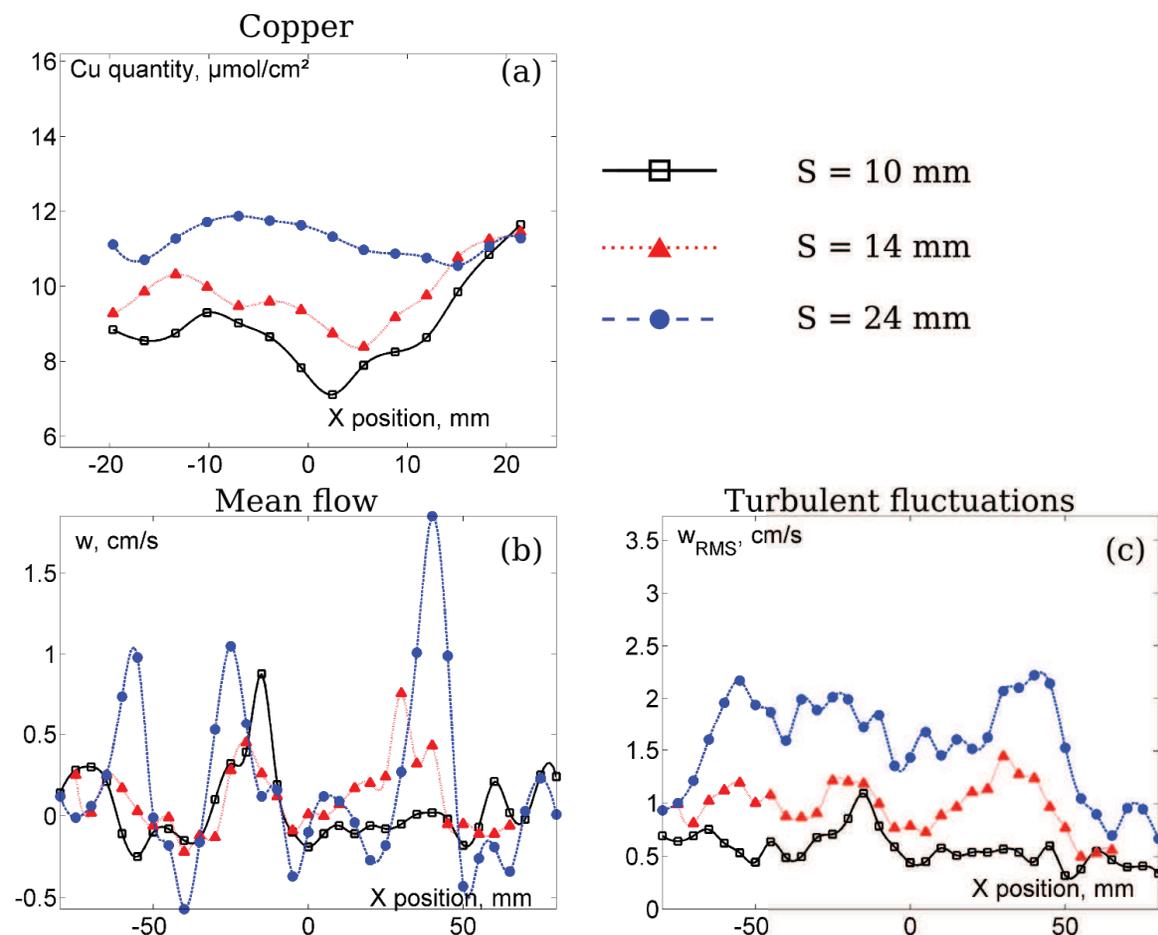
$$J_c = \frac{nFDC_B}{\delta} \tag{6}$$

Fig. 4. Effect of the stroke on copper deposition and flow parameters

δ is itself linked to the Sherwood number $Sh = l_B/\delta$, where l_B is the typical size of the eddies. For this system, we assumed that $l_B = g$ because the eddies are confined between the comb and the cathode, therefore the largest possible size for the eddies is g.

The Sherwood number is linked to the Reynolds and Schmidt numbers (equation 7):

$$Sh = \alpha Re^{1/2} Sc^{1/3} \tag{7}$$

$$Sh = \left(\frac{M}{w}\right)^{1/4} \cdot \left(\frac{Sf(h+g)}{\nu}\right)^{1/2} \cdot \left(\frac{\nu}{D}\right)^{1/3} \tag{8}$$

Combining eq. 6 with eq. 8 and taking $l_B = g$ yields:

$$J_c = n\mathrm{F}C_B \left(\frac{M}{w}\right)^{1/4} \cdot \frac{[Sf(h+g)]^{1/2}}{g} \cdot D^{2/3} \cdot \nu^{-1/6} \tag{9}$$

The experimental deposition current is plotted as a function of the geometric deposition current J_C in fig. 5. The measured current density is indeed proportional to the geometric current density. That means that the number $L = (M/w)^{1/4} \cdot [Sf(h+g)]^{1/2}/g$ is a geometric control parameter for the deposition current: for higher values of L, the current density gets higher.
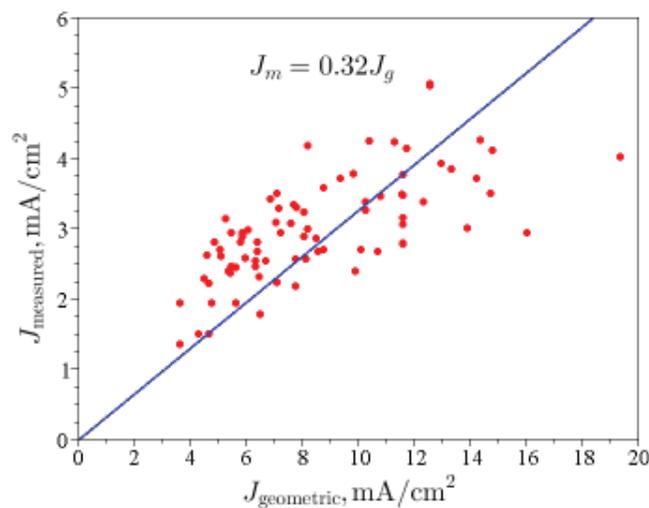

Fig. 5. Measured deposition current J_{measured} is plotted as a function of the geometric deposition current $J_{\mathrm{geometric}}$

4.4 Homogeneity control

To define a control parameter for the homogeneity of the electrodeposited layer the standard deviation of the electrodeposited layer versus each relevant non-dimensional parameter has been plotted separately. This allowed the design of a control parameter depending on the non-dimensional stroke, the proximity ratio and a modified Reynolds Number

$$K = \frac{S}{M} \cdot \frac{g}{h} \cdot \frac{fSh}{\nu} \tag{10}$$

Figure 6 shows the standard deviation of copper in Cu-Ni layers σ_{Cu} versus the non-dimensional parameter K. The variation is monotonous: the standard deviation σ_{Cu}

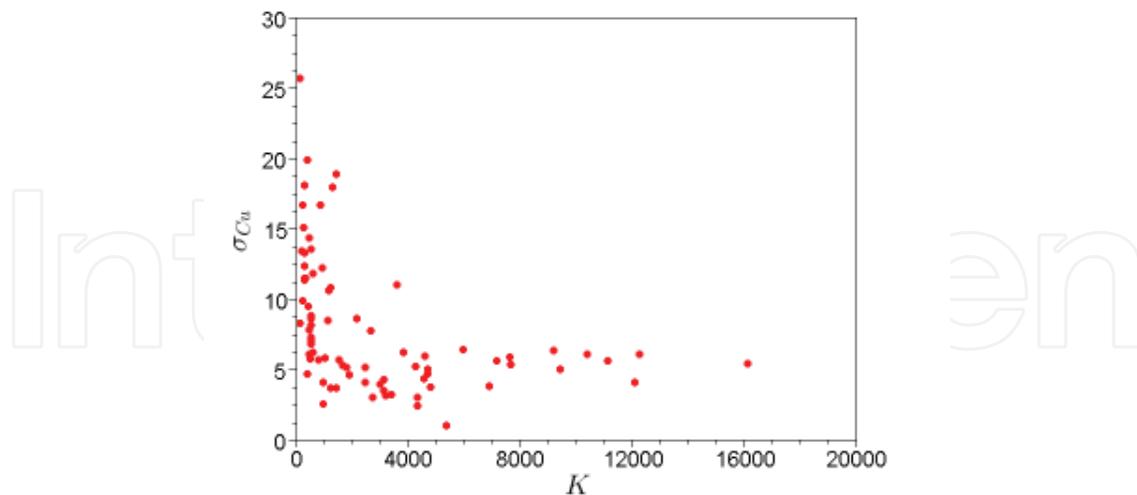Fig. 6. σ_{Cu} in Cu-Ni electrodepositions vs. non-dimensional control parameter K.

decreases when K increases, meaning that the homogeneity of the electrodeposition increases when K increases.

The minimum standard deviation of Cu quantity obtained for this comb-like system was 1.07 % on 5 x 5 cm². The experimental conditions for this electrodeposition were M = 9 mm, h = 4 mm, w = 1 mm, g = 25 mm, S = 24 mm, f = 5.4 Hz, and the tooth section was rectangular. This value can be compared to the homogeneity of Fe-Ni layers synthesized in paddle-cell industrial electrolysers: Andricacos et al. (1994) report that the normalized standard deviation on circular wafers (diameter 30 cm) can be as low as 1.38 % for the Fe-Ni thickness and 0.86 % for the Fe content of the Fe-Ni layer. The homogeneity of electrodeposited layers performed in comb-like reactors are therefore comparable to the ones performed in industrial paddle-cell electrolysers used for electronic applications.

4.5 Interactions between the two control parameters

The two previously defined two control parameters allow the optimization of Cu-Ni homogeneity and the deposition current. As the control parameters K and L are made out of the same geometrical parameter, their relashionship has been studied. Figure 7 shows the geometrical deposition current J versus the homogeneity control parameter K.

For K > 5000 corresponding to homogeneous deposition (see figure 6), J can take the whole range of possible values. That means that it is possible to choose any deposition current and still perform homogeneous electrodeposition, which is particularly interesting for industrialization of such processes.

5. Results: control parameters of Cu-Ni electrodeposition in jet systems

5.1 Mixing and transport in randomly firing jet systems

The turbulence-generating device using a randomly firing jet array has been presented in (Variano et al., 2004; Variano & Cowen, 2008), where an array of jets fires in the same direction at the same discharge (volume of fluid per unit of time), randomly switched on and off. 1D jet arrays are typically holed pipes, and 2D jet arrays are typically holed plates. A definition diagram of a jet array is shown in figure 8. The stirring tank used in this study and related electrochemical methods are described in (Delbos et al., 2009a;b).
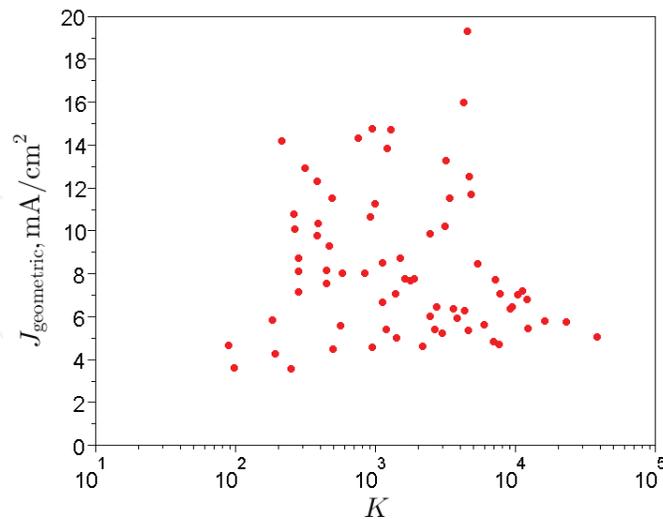
Fig. 7. Geometric deposition current $J_{\mathrm{geometric}}$ vs homogeneity control parameter K

Previous studies Delbos et al. (2009b;a); Variano & Cowen (2008) showed that the important parameters for turbulence control in such systems were mainly the distance between the jets M, and the cathode z_d, as well as the momentum source fraction, which is the ratio of time of firing and time of sleep. However, no relationship between current density and geometrical parameters of the jet array has been reported yet. Furthermore, no information has been found related to the spatial variations of δ and its effects on the homogeneity of the electrodeposited layer in such systems.

The following findings are based on the experimental results obtained from (Delbos et al., 2009b;a), which also describe the experimental details of their experiments, which will not be repeated here.

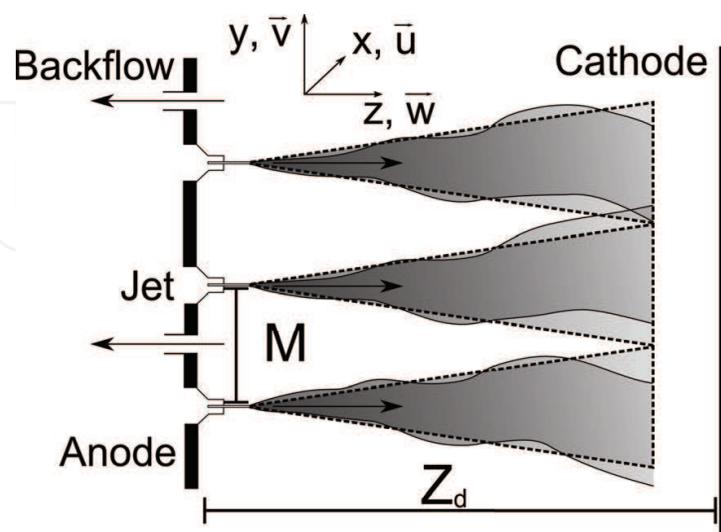The operating conditions of the jet systems are described in table 4

Fig. 8. Definition diagram of a jet array, showing the single jet discharges and their merging.

Parameter	Range
W_0 (m/s)	$2.6, 7.4$
d (mm)	$0.7 - 1$
z_m (mm)	$60 - 230$
M (mm)	$18, 29, 45$
$\phi_j (\%)$	$50, 100$

Table 4. Hydrodynamical conditions random jet array system. See List of symbols and figure 8

5.2 Non-dimensional parameters

As for the comb systems, first the non-dimensional geometrical parameters that control the flow characteristics are defined:

– Merging ratio
  As mentioned in (Delbos et al., 2009a;b), the merging length is a predominant factor for homogeneity: if the merging ratio z_d/L is smaller than 1, the jets are not merged and impinging patterns appear on electrodeposited layers. When the jet raster is different in horizontal and vertical directions, there are two merging lengths L_v and L_h, and therefore both corresponding merging ratios are used for the design of non-dimensional parameters.

– Reynolds number
  The Reynolds number of the individual jets was chosen to describe the turbulence intensity.

$$Re = \frac{W_0 d}{\nu} \tag{11}$$

In these set of experiments, the temperature could not be well controlled but was measured. The variation of the kinematic viscosity with temperature was therefore taken into account. The variation of water dynamic viscosity was taken from (Likhachev, 2003):

$$\eta = \eta_0 \exp \frac{E}{R(T + T_0)} \tag{12}$$

where $\eta_0 = 2.414 \cdot 10^{-5}$ Pa.s, R = 8.314 J.K^{-1}.mol^{-1}, E = 2060 J.mol^{-1}, $T_0 = 133.15°$C, T is in °C. The variation of volumic mass is described in (McCutcheon et al., 1993):

$$\rho(T) = 1000 \cdot (1 - \frac{(T + 288.9414) \cdot (T - 3.9863)^2}{508923 \cdot (T + 68.12963)}) \tag{13}$$

where T is in °C

– Nondimensional turbulence decay ratio
  For perforated plates, the turbulence decay is proportional to the inverse of the distance from the turbulence generating device to the power 3/2 ($u_{RMS} \propto z^{-3/2}$)) (Thompson & Turner, 1975). As the turbulence intensity decreases with the distance from the turbulence generation system, the stirring efficiency decreases with the distance from the nozzle. We propose a nondimensional turbulence decay ratio $(\ell/z_d)^{3/2}$ (where ℓ is the size of the jet array) to quantify the decreased homogeneity due to the turbulence decay:

– Randomization coefficient

Finally, the randomization had to be taken into account. The influence of the source fraction $\phi_j = \mu_{on}/(\mu_{off} + \mu_{on})$ on the turbulence generation was studied in (Variano & Cowen, 2008). This study shows that the optimal value of ϕ_j for turbulence generation is 12.5 %. In the case of this study, the source fraction was 50 % in the random case, and 100 % in the continuous case. A coefficient k was designed so as to quantify the influence of random and non-random injection, and the most fitting results, resulting from euristic methods, are:

k = 0.45 when the injection is continuous

k = 0.80 when the injection is random

5.3 Deposition current control

For the jet system, eq.8 did allow us to describe a geometric control parameter of the system. A similar relationship is proposed, which was found through heuristic methods:

$$Sh = \frac{l_B}{\delta} = \alpha Re^{0.1} Sc^{-0.9} \tag{14}$$

where $l_B = \ell$: the eddy size l_B is the dimension of the jet array ℓ (a result described in (Delbos et al., 2009b)), $\alpha = [(L_h L_v)/z_d^2]^{0.1}$

Combining eq. 6 with eq.14 yields:

$$J_c = nFC_B \left(\frac{L_h L_v}{z_d^2} \right)^{0.1} \cdot \frac{(W_0 d)^{0.1}}{\ell} \cdot \frac{D^{1.9}}{\nu(T)} \tag{15}$$

The experimental deposition current is plotted as a function of the geometric deposition current J_C in fig. 9. The measured current density is indeed proportional to the geometric current density. That means that the number $L = \left(\frac{L_h L_v}{z_d^2} \right)^{0.1} \cdot \frac{W_0 d}{\ell}$ is a geometric control parameter for the deposition current: for higher values of L, the current density gets higher. Surprisingly, the type of injection (random or continuous) does not play any role in the value of the deposition current. In (Delbos et al., 2009b), we showed that the random injection increased the turbulent velocity but decreased the mean flow. It could be that these effects balance each other, causing random and continuous injection to yield similar values of current density.

5.4 Homogeneity control

This control parameter was built with the same method used for the comb system. The proposed nondimensional control parameter is:

$$K = \underbrace{k}_{(1)} \underbrace{\frac{z_d}{L_v} \frac{z_d}{L_h}}_{(2)} \underbrace{\left(\frac{\ell}{z_d} \right)^{3/2}}_{(3)} \underbrace{\frac{W_0 d}{\nu(T)}}_{(4)} \tag{16}$$

where (1) is the randomization coefficient, (2) are the merging ratios, (3) is the turbulence decay ratio, and (4) is the Reynolds number. The choice of 1 as the exponent for all the member except the turbulence decay ratio yielded the best results in term of monotony of the $K - \sigma$ plot.

Figure 10 shows the standard deviation of copper in Cu-Ni layers σ_{Cu} versus the nondimensional parameter K. The variation is monotonous: the standard deviation σ_{Cu}
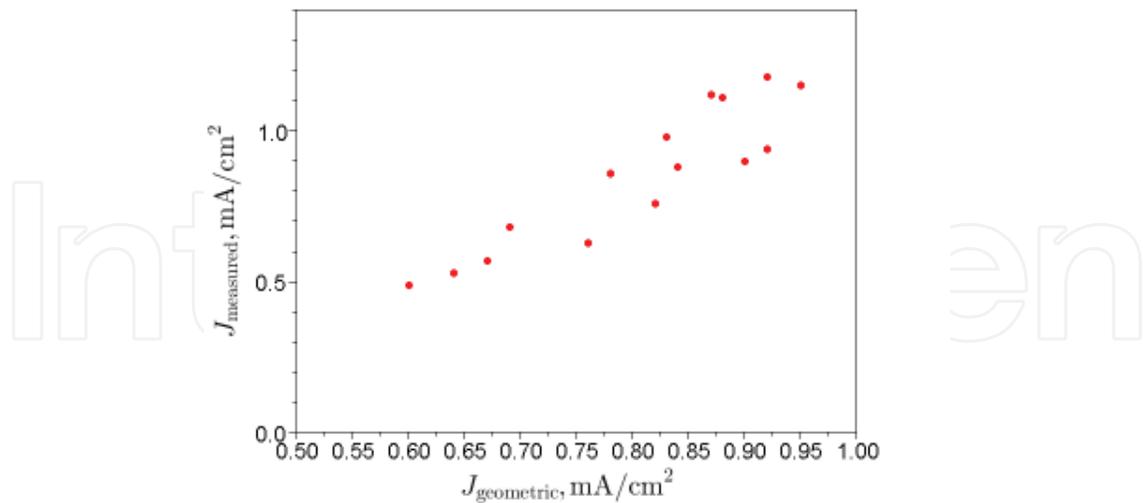
Fig. 9. Measured deposition current is plotted as a function of the geometric deposition current J_C

decreases when K increases, indicating that the homogeneity of the electrodeposited layer increases when K increases. Random injection generates more homogeneous deposition, high values of distance nozzle-to-cathode, initial velocity, and low values of merging distance (and therefore low values of jet mesh) are also helpful for homogeneous depositions.

5.5 Interactions between the two control parameters
The methodology used for the comb was also used for the jet array. The figure 11 shows the geometric current as a function of K. It shows that for high values of K yielding the best homogeneity, a wide range of values of J can be chosen.
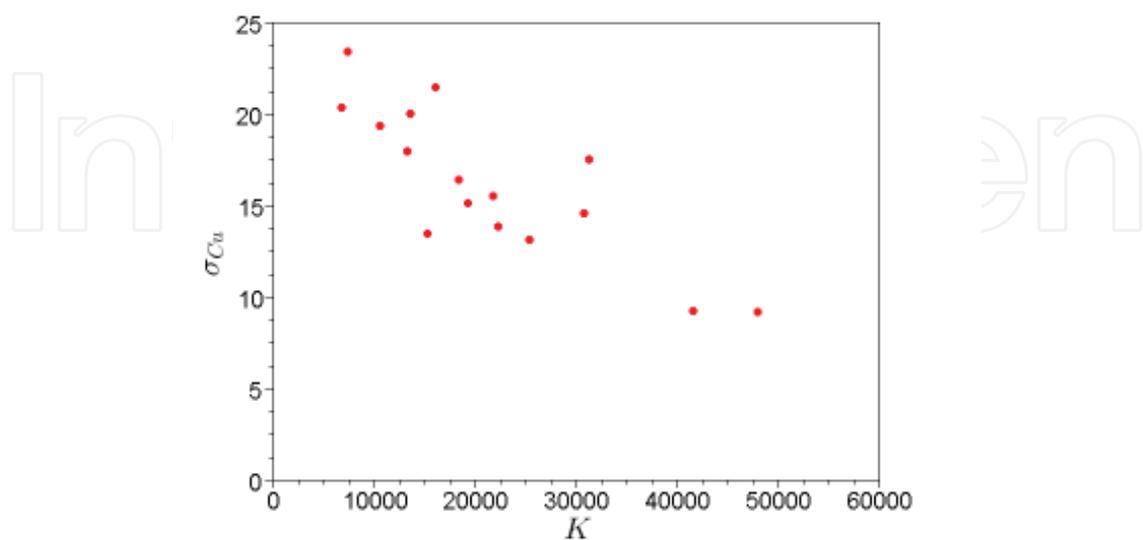
Fig. 10. σ_{Cu} in Cu-Ni electrodepositions vs. nondimensional control parameter K
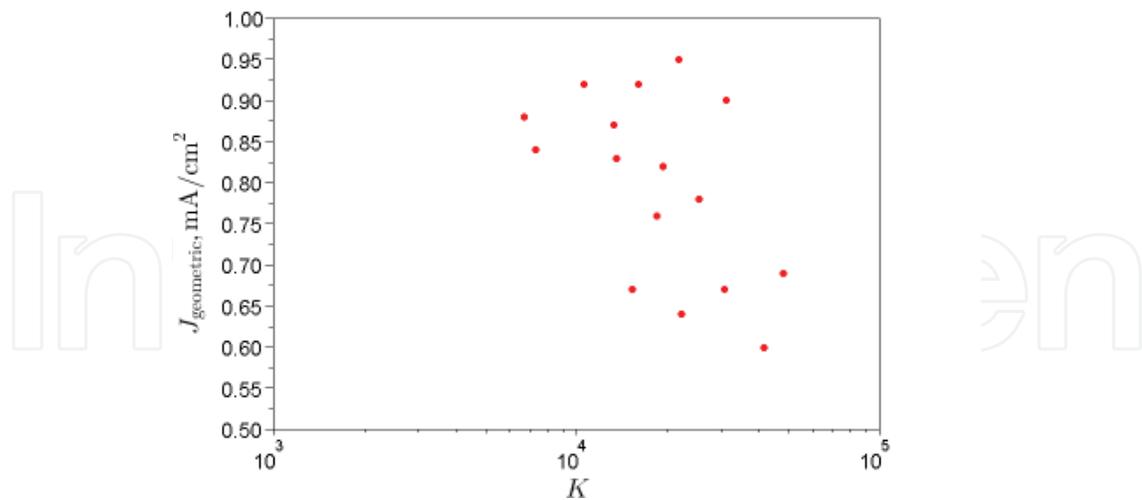
Fig. 11. J vs. K for the jet array system

6. Conclusion

In the microelectronics industry, the paddle-cell is widely used for enhancing mass transfer in diffusion controlled plating of alloys. In this paper two alternative stirring sytems, the comb-like system and the random jet array, are studied in details. In particular two control parameters are developed. Electrodeposited layers mappings were linked to LDV measurements of the flow velocity in order to the find geometrical parameters relevant to electrodeposition control. From these experiments two control parameters for each system were designed. They allow comb and random jet array systems operators to control the mean deposition current and the homogeneity of the electrodeposited layer. More generaly, these parameters control the mass transfer in these systems.

7. List of symbols

δ	diffusion layer thickness (mm)
ν	kinematic viscosity (m^2/s)
ϕ_j	momentum source ratio
ρ_{ca}	resistivity of the cathode (Ω.m)
σ	standard deviation
C	concentration (mol/L)
D	Molecular diffusion coefficient (m^2/s)
d	diameter of the jet nozzles (mm)
H	dimension of the cell in the direction perpendicular to the cathode (mm)
f	stirring frequency (Hz)

| f_v	vortex shedding frequency (Hz)
g	distance between cathode and paddle or comb (mm)
h	height of paddle or height of comb teeth (mm)
i_{Cu}	copper partial current (A/cm^2)
i_L	diffusion-limited current (A/cm^2)
K	Homogeneity control parameter
L	Current control parameter
ℓ	dimension of the jet array (mm)
L	dimension of the cell in the direction parallel to the cathode (mm)
L_h	horizontal merging length (mm)
L_v	vertical merging length (mm)
LDV	Laser Doppler Velocimetry
l_B	advection lengthscale (mm)
M	distance between the teeth of the comb or distance between the nozzles (mm)
n_Cu	Copper quantity in the electrodeposited layer (mol/mm^2
Re	Reynolds number
RMS	Root Mean Square deviation
S	Stroke (mm)
Sc	Schmidt number
Sh	Sherwood number
St	Strouhal number
u,w	Flow velocity in the directions horizontal, parallel to the cathode and perpendicular to the cathode (mm/s)
u_B	typical eddy size (mm)
$\overline{u},\overline{w}$	Mean flow velocity (mm/s)
$u_{\text{RMS}}, w_{\text{RMS}}$	turbulent fluctuations (mm/s)
V	velocity of the paddle or velocity of the comb (mm/s)
W_0	initial velocity of the jets (mm/s)
w	width of paddle or width of comb teeth (mm)
XRF	X-Ray Fluorescence
x,y,z	coordinates, horizontal, parallel to the cathode, vertical, and perpendicular to the cathode (mm)
z_d	distance between nozzles and cathode (mm)
z_e	number of electrons in the electrochemical reaction (mm)
z_m	distance between the cathode and the LDV measurements (mm)

8. References

Andricacos, P., Branger, M., Browne, R. M., Dukovic, J. O., Fu, B. W. B., Hitzfeld, R. W., Flotta, M., McKenna, D. R., Romankiw, L. T. & Sahami, S. (1994). Multi-compartment electroplating system. US patent No 5312532, IBM.

Bard, A. J. & Faulkner, L. R. (2001). *Electrochemical methods: fundamentals and applications*, John Wiley & Sons, Inc.

Brumley, B. H. & Jirka, G. H. (1988). Air water transfer of slightly solulble gases – turbulence, interfacial processes and conceptual models, *Physicochemical hydrodynamics* 10(3): 295–319.

Cussler, E. L. (1997). *Diffusion - Mass transfer in fluid systems, 2nd edition*, Cambridge University Press.

Datta, M. & Landolt, D. (2000). Fundamental aspects and applications of electrochemical microfabrication, *Electrochemical Acta* 45: 2535–2558.

Delbos, S. (2008). *Électrodépot de Cu-In-Se contrôlé par turbulence pour la production de cellules solaires*, PhD thesis, Université Pierre et Marie Curie Paris.

Delbos, S., Grand, P.-P., Chassaing, E., Weitbrecht, V., Bleninger, T., Jirka, G. H., Lincot, D. & Kerrec, O. (2009). Application of randomly firing jet arrays for electrodeposition, *Journal of the Electrochemical Society* 156(11): 161–166.

Delbos, S., Weitbrecht, V., Bleninger, T., Grand, P.-P., Chassaing, E., Lincot, D., Kerrec, O. & Jirka, G. H. (2009). Homogeneous turbulence at an electrodeposition surface induced by randomly firing jet arrays, *Experiment in Fluids* 46(6): 1105–1114.

Henninot, C. (1999). *Codéposition électrochimique d'un alliage*, PhD thesis, INPL ENSIC Nancy.

Keigler, A., Liu, Z., Harrell, J. & Wu, Q. (2005). Method and apparatus for fluid processing a workpiece. International patent No 2005/042804A3, NEXX Systems, Inc.

Likhachev, E. (2003). Dependence of water viscosity on temperature and pressure, *Technical Physics* 48(4): 514–515.

Lincot, D., Guillemoles, J.-F., Taunier, S., Guimard, D., Sicx-Kurdi, J., Chomont, A., Roussel, O., Ramdani, O., Hubert, C., Fauvarque, J.-P., Bodereau, N., Parissi, L., Panheleux, P., Fanouillère, P., Naghavi, N., Grand, P.-P., Benfarah, M., Mogensen, P. & Kerrec, O. (2004). Chalcopyrite thin film solar cells by electrodeposition, *Solar Energy* 77: 725–737.

Mandin, P., Cence, J.-M., Fabian, C., Gbado, C. & Lincot, D. (2007). electrodeposition process modeling using continuous and discrete scales., *Computer and Chemical engineering* 31: 980–992.

McCutcheon, S. C., Martin, J. L. & Barnwell, T. (1993).

McHugh, P. R., Wilson, G. J., Woodruff, D. J., Zimmerman, N. & Erickson, J. J. (2005). Reactor having multiple electrodes and/or enclosed reciprocating paddles, and associated methods. US patent No 2005000817A1, Semitool, Inc.

Ollivier, A., Muhr, L., Delbos, S., Grand, P. P., Matlosz, M. & Chassaing, E. (2009). Copper–nickel codeposition as a model for mass-transfer characterization in copper-indium-selenium thin-film production, *Journal of Applied Electrochemistry* 39(12): 2337–2344.

Powers, J. V. & Romankiw, L. T. (1972). Electroplating cell including means to agitate the electrolyte in laminar flow. US patent No 3652442, IBM.

Rice, D. E., Sundstrom, D., McEachen, M. F., Klumb, L. A. & Talbot, J. B. (1988). *J. Electrochem. Soc* 135(11): 2777–2780.

Schwartz, D. T., Higgins, B. G. & Stroeve, P. (1987). *J. Electrochem. Soc* 134(7): 1639–1645.

Tennekes, H. & Lumley, J. L. (1972). *A first course in turbulence*, The MIT Press.

Thompson, S. M. & Turner, J. S. (1975). Mixing across an interface due to turbulence generated by an oscillating grid, *Journal of Fluid Mechanics* 67: 349.

Tzanavaras, G. & Cohen, U. (1995). Precision high rate electroplating cell and method. US patent No 5421987.

Variano, E. A., Bondenschatz, E. & Cowen, E. A. (2004). A random synthetic jet array driven turbulence tank, *Experiments in fluids* 37(4): 613–615.

Variano, E. A. & Cowen, E. A. (2008). A random-jet-stirred turbulence tank, *Journal of Fluid Mechanics* 640: 1-32.

Wilson, G. & McHugh, P. (2005). Unsteady numerical simulation of the mass transfer within a reciprocating paddle electroplating cell, *J.Electrochem. Soc* 152(6): 356–365.

Wu, B. Q., Liu, Z., Keigler, A. & Harrell, J. (2005). Diffusion boundary layer studies in an industrial wafer plating cell, *journal of the Electrochemical Society* 152(5): 272–276.
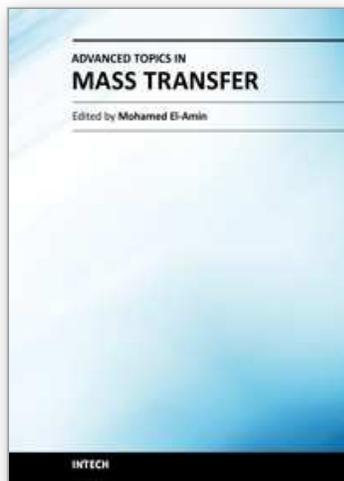
Advanced Topics in Mass Transfer

Edited by Prof. Mohamed El-Amin

ISBN 978-953-307-333-0

Hard cover, 626 pages

Publisher InTech

Published online 21, February, 2011

Published in print edition February, 2011

This book introduces a number of selected advanced topics in mass transfer phenomenon and covers its theoretical, numerical, modeling and experimental aspects. The 26 chapters of this book are divided into five parts. The first is devoted to the study of some problems of mass transfer in microchannels, turbulence, waves and plasma, while chapters regarding mass transfer with hydro-, magnetohydro- and electro- dynamics are collected in the second part. The third part deals with mass transfer in food, such as rice, cheese, fruits and vegetables, and the fourth focuses on mass transfer in some large-scale applications such as geomorphologic studies. The last part introduces several issues of combined heat and mass transfer phenomena. The book can be considered as a rich reference for researchers and engineers working in the field of mass transfer and its related topics.

INTECH
open science | open minds